

Sampling of the Wigner function adapted to time-multiplexed detection of photon statistics

K Laiho, M Avenhaus, K N Cassemiro, and Ch Silberhorn

Max Planck Research Group, Günther-Scharowsky-straße 1/Bau 24, 91058 Erlangen, Germany

E-mail: klaiho@optik.uni-erlangen.de

Abstract. We investigate the capabilities of loss-tolerant quantum state characterisation based on photon-number resolving detectors. Our emphasis lies on constructing the Wigner function of non-Gaussian Fock states with highly non-classical negative values around the origin of the phase space. We employ the idea of sampling the Wigner function point by point via photon parity measurements instead of using conventional homodyne tomography. Different regions in the phase space can be probed by applying appropriate displacements to the studied quantum state, which requires an overlap of the quantum signal with a weak coherent reference beam. Our results show that high losses in the experimental realisation can be tolerated for a defined parameter range enabling a reliable reconstruction of the photon number statistics and its characteristic oscillations. Further, we analyse the impact of imperfect mode overlap between signal and reference beam. We find that, in contrast to homodyne tomography, we can clearly distinguish a mode mismatch from losses and inefficiencies caused by detectors.

PACS numbers: 03.65.Wj, 42.50.-p, 42.50.Ar

1. Introduction

Optical quantum information processing (QIP) can be divided in general into two different branches with specific protocols and realisations for quantum computing and communication applications. On the one hand, there are protocols based on discrete variables, where information is encoded on quantum bits (qubits) such as single photons. On the other hand, there exist QIP protocols based on continuous variables (CV), which typically employ Gaussian states such as coherent or squeezed light. CV schemes are often less demanding in terms of state preparation, however CV entanglement distillation is not possible without non-Gaussian operations or non-Gaussian states [1, 2]. Since quantum repeaters rely on entanglement distillation, this severely affects usual CV quantum communication over long distances.

Hence, non-Gaussian states and non-Gaussian operations play an important role in both, CV and qubit based QIP applications and an accurate characterisation of

their properties is paramount. The most fundamental non-Gaussian states are Fock states, which exhibit an exact photon number in a single mode. Experimentally, the engineering and characterisation of Fock states containing only a single energy quantum or two quanta is challenging but it has been demonstrated recently [3, 4, 5, 6]. In phase space the Wigner function completely defines any arbitrary quantum state by a quadrature representation and Gaussian states exhibit positive distributions. Though for non-Gaussian states, in particular for Fock states with non-zero photon number, the Wigner function presents negative values as a genuine quantum feature. A usual measurement of the Wigner function is carried out by employing conventional homodyne detection followed by a tomographic technique [7].

Homodyne detection is implemented using conventional photo-diodes and a balanced beam splitter, where the weak quantum signal is overlapped with a bright reference beam—typically referred to as the local oscillator [8]. After their interference, the differences of the photon currents of the two output channels are recorded, which corresponds to different quadrature measurements according to the relative phases between signal and local oscillator. This procedure intrinsically introduces a filtering operation of the quantum signals, since photons that do not spectrally overlap with the local oscillator are not detected. Thus, this effect can not be distinguished from losses, which in turn causes an inefficient calibration of the detection efficiency. Another drawback in this method is the fact that homodyne tomography is always an indirect state characterisation: the Wigner function can be constructed only after intricate computational back-projection and the photon statistics has to be recovered by more involved means, for detailed description see e.g. [9].

A more direct characterisation of the Wigner function can actually be done if a photon number resolving detector is available. The value $W(\alpha)$ of a Wigner function at a given position α of the phase space ($\alpha \in \mathcal{C}$) is equal to the average value of the photon number parity ($\hat{\Pi}$) operating on a quantum signal state displaced by the amount of $-\alpha$ [10]. As the observable $\hat{\Pi}$ has the Fock states as eigenfunctions, its expectation value can be directly inferred from a complete determination of the photon number distribution [11, 12]. In this paper we call this method *sampling technique*. As opposed to tomography, the Wigner function is probed point by point in phase space. A first experiment, which demonstrated the principle of this approach, has been successfully carried out for coherent states in 1999 [13]. Nevertheless, for more interesting states with non-Poissonian distributions, the requirement of measurements with photon number resolution has severely limited the usage of the method. In the case of experiments dealing with interactions between photons and atoms, the latter enables to extract the value of $\langle \hat{\Pi} \rangle$ from observed Ramsey fringes [14, 15].

Recently, new strategies for measuring light with photon number resolution have been developed, allowing a more intensive exploration and characterisation of quantum states, see e.g. [16]. One of them, applicable for pulsed light, is a time multiplexed detector (TMD), which is especially attractive for QIP due to its simple implementation and operation [17, 18]. A TMD distributes a pulse of light into temporally adjacent

pulses, which are subsequently measured with on-off detectors, namely avalanche photo diodes (APDs). The recorded data does not directly correspond to the photon statistics themselves, but to the so-called click statistics. In a loss-tolerant photon counting setup the photon statistics can be revealed by taking into account the detection losses and the classical distribution of photons in time domain. The first experiment using this concept has been reported in 2005, demonstrating a reliable loss calibration, which enabled the conditional preparation and verifications of number states with nearly completely suppressed vacuum contributions [19]. In 2008 the TMD has also been successfully applied in the detection of multimode statistics of twin-photons generated by parametric down-conversion (PDC), which confirmed the suitability of loss-tolerant state characterisation for determining photon statistics [20].

In this work we simulate an experiment that aims at the characterisation of Fock states via the sampling technique. In a related work, Banaszek and Wodkiewicz analysed how reliable the Wigner function reconstruction of a degraded quantum signal is, i.e. subject to the effect of statistical errors and losses [21]. We follow their steps in the context of adding recent developments in the analysis of experimental imperfections. We explicitly consider for the first time the use of the TMD device for achieving the photon number resolution and analyse in detail the influence of mode mismatch and its distinct signature in the detected photon statistics.

This paper is organised as follows: In Sec. 2 we introduce a scheme for sampling the Wigner function via displacement operations and photon counting. We investigate the influence of implementing the displacement with an asymmetrical beam splitter and compare the result with a model that considers separately losses and ideal displacements for the single photon Fock state. In Sec. 3 we briefly review the properties of a TMD and explain how to reconstruct the Wigner function of quantum states using click statistics. In Sec. 4 we employ Monte Carlo simulations to analyse the reliability of the sampling technique in the high loss regime, showing how efficiently the Wigner function characteristics can be recovered from the response of the TMD. In the following Sec. 5 we introduce a simple model to study the effect of imperfect mode overlap and show that the matching degree can be estimated from the experimental data. Contrarily to usual homodyne detection, this method allows a more sophisticated analysis of the quantum signal: detector inefficiencies do not degrade the state characterisation and multimode spectral structures that are not matched by the single mode reference beam can be recognised from the measured statistics. The mode overlap presents distinct features when compared to the behaviour caused by losses. Finally, in Sec. 6 we conclude and highlight the main findings of our investigations.

2. Measurement of the Wigner function by sampling technique

Mathematically, the sampling method is based on evaluating the Wigner function at the origin of the phase space by taking the mean value of the photon number parity

operator $\hat{\Pi}$ [11, 12],

$$W(0) = \frac{2}{\pi} \text{Tr}(\hat{\rho} \hat{\Pi}). \quad (1)$$

As the Fock states $|n\rangle$ are the eigenstates of the photon number parity operator (with eigenvalues $(-1)^n$), a natural representation for the density matrix is $\hat{\rho} = \sum \rho_{mn} |m\rangle \langle n|$. In this way Eq. (1) simplifies to

$$W(0) = \frac{2}{\pi} \sum_n (-1)^n \rho_{nn}. \quad (2)$$

Since the projection onto the photon number basis always erases the information about coherences of the state, the parity measurement gives the value of the Wigner function only at one single point of phase space. Nevertheless, the whole Wigner function can be constructed by applying appropriate displacements to the state. To access the value $W(\alpha)$ we have to displace the state by the quantity $-\alpha$, which corresponds to applying the operator $\hat{D}(-\alpha) = \hat{D}^\dagger(\alpha)$ to the original signal state. This yields,

$$W(\alpha) = \frac{2}{\pi} \text{Tr}(\hat{D}^\dagger(\alpha) \hat{\rho} \hat{D}(\alpha) \hat{\Pi}). \quad (3)$$

Physically, the displacement operation can be well approximated by the action of a highly asymmetrical beam splitter with transmission $T \approx 1$, which is used to superimpose the quantum signal of interest with a strongly attenuated coherent reference beam $|\beta\rangle$ [22]. In Fig. 1 we illustrate a scheme for modelling the implementation of the sampling technique. In addition to a displacement, which is realised by the first beam splitter with transmission T , we also include a loss element represented by a second beam splitter with transmission η in order to account for the limited quantum efficiency of detectors.

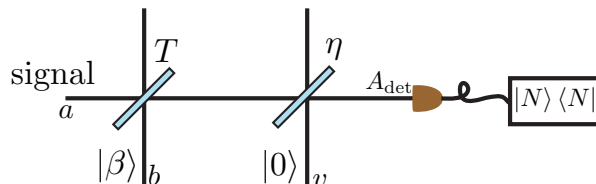


Figure 1. Scheme for modelling the implementation of the sampling technique. The first beam splitter with transmission T displaces the quantum signal, while the second one with transmission η is used to model losses.

We can easily see the action of this network on a given input field by calculating the evolution of the annihilation operator \hat{a} . The beam splitter operator is a unitary transformation $\hat{\mathcal{U}}$ relating the input and output modes via matrix \mathcal{U}

$$\begin{pmatrix} \hat{A}_{out} \\ \hat{B}_{out} \end{pmatrix} = \mathcal{U} \begin{pmatrix} \hat{a}_{in} \\ \hat{b}_{in} \end{pmatrix}. \quad (4)$$

In the Heisenberg picture the input modes \hat{a}_{in} and \hat{b}_{in} can be expressed in terms of the output modes by using \mathcal{U}^{-1} , which gives

$$\begin{aligned}\hat{a}_{in} &= \sqrt{T}\hat{A}_{out} - \sqrt{1-T}\hat{B}_{out} \quad \text{and} \\ \hat{b}_{in} &= \sqrt{1-T}\hat{A}_{out} + \sqrt{T}\hat{B}_{out}.\end{aligned}\quad (5)$$

Using the relation in Eq. (4), we obtain for the mode at the detector

$$\begin{aligned}\hat{A}_{det} &= \sqrt{\eta T}\hat{a} + \sqrt{\eta(1-T)}\hat{b} + \sqrt{1-\eta}\hat{v} \\ &= \sqrt{\eta T}\left(\hat{a} + \sqrt{(1-T)/T}\hat{b}\right) + \sqrt{1-\eta}\hat{v}.\end{aligned}\quad (6)$$

According to Eq. (6) the efficiency of the network is ηT , and the displacement set by the reference beam is modified by the factor $\sqrt{\frac{1-T}{T}}$.

In order to analyse the performance of a displacement implemented by a highly asymmetrical beam splitter, we evaluate the state's photon number distribution for two idealised cases, as illustrated in Fig. 2 and described in the next two paragraphs. First we consider the network shown in Fig. 2a representing a lossless channel followed by displacement using a beam splitter. In the following paragraph, we consider a lossy channel followed by ideal displacement (Fig. 2b) and compare the results. Our derivations prove that for an incoming single photon Fock state, the photon number distribution on both descriptions coincide if the ideal displacement α is chosen appropriately.

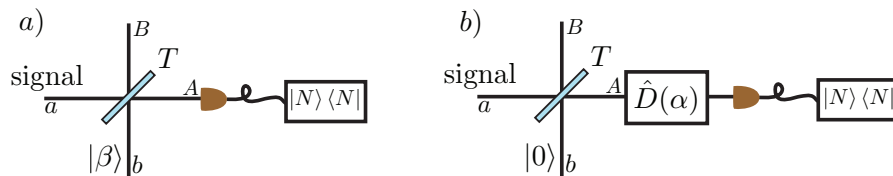


Figure 2. State characterisation models with a) asymmetrical beam splitter and b) loss element in front of an ideal displacement. The action of the models corresponds to each other for a single photon Fock state.

A) Lossless channel followed by displacement via asymmetrical beam splitter

Let us assume lossless detection ($\eta = 1$) and calculate the elements of the density matrix of the displaced state. The displacement is implemented by a beam splitter with transmittance T , and the quantum signal and the reference beam are launched in it through the ports a and b respectively. The signal at the output port A is detected while the one at port B is neglected, i.e. we are interested in the reduced density matrix $\hat{\rho}_A$ given by tracing out the undetected arm B from the two-mode state $\hat{\rho}_{AB}$. The element ρ_{NM} of $\hat{\rho}_A$ is given by

$$\rho_{NM} = Tr_{AB} \{ \hat{\rho}_{AB} |M\rangle_A \langle N| \} = \sum_B \langle B|_A \langle N| \hat{\rho}_{AB} |M\rangle_A |B\rangle_B. \quad (7)$$

We can evaluate Eq. (7) using the identity relation $\hat{U}^\dagger \hat{U} = \mathbf{1}$. This enables to express the density matrix $\hat{\rho}_{AB}$ in terms of the incoming fields,

$$\hat{U}^\dagger \hat{\rho}_{AB} \hat{U} = \hat{\rho}_{ab} = \hat{\rho}_a \otimes |\beta\rangle_b \langle\beta|, \quad (8)$$

and the evolution of the number states $|M\rangle_A |B\rangle_B$ is easily calculated [similar to Eq. (5)],

$$\begin{aligned} \hat{U}^\dagger |M\rangle_A |B\rangle_B &= \hat{U}^\dagger \left[\frac{1}{\sqrt{M!}} (A_{out}^\dagger)^M \frac{1}{\sqrt{B!}} (B_{out}^\dagger)^B |0\rangle_{AB} \right] \\ &= \frac{1}{\sqrt{M!B!}} \left(\sqrt{T} \hat{a}_{in}^\dagger + \sqrt{1-T} \hat{b}_{in}^\dagger \right)^M \\ &\quad \times \left(-\sqrt{1-T} \hat{a}_{in}^\dagger + \sqrt{T} \hat{b}_{in}^\dagger \right)^B |0\rangle_{AB}. \end{aligned} \quad (9)$$

Using Eqs. (8) and (9) together with the eigenvalue relation $\hat{b}_{in} |\beta\rangle_b = \beta |\beta\rangle_b$ and writing $\rho_a = \sum c_{mn} |m\rangle_a \langle n|$, Eq. (7) can be evaluated:

$$\rho_{NM} = \sum_{mn} c_{mn} \sum_B f(m, \beta, N, B)^* f(n, \beta, M, B), \quad (10)$$

where the function f is given by

$$\begin{aligned} f(n, \beta, M, B) &= \frac{b \langle \beta | 0 \rangle_b}{\sqrt{M!B!}} \langle n | \left(\sqrt{T} \hat{a}_{in}^\dagger + \sqrt{1-T} \beta^* \right)^M \\ &\quad \times \left(-\sqrt{1-T} \hat{a}_{in}^\dagger + \sqrt{T} \beta^* \right)^B |0\rangle_a. \end{aligned} \quad (11)$$

The matrix element in Eq. (11) can be evaluated with the help of the binomial expansion

$$\begin{aligned} f(n, \beta, M, B) &= \frac{\sqrt{n!}}{\sqrt{M!B!}} e^{-\frac{|\beta|^2}{2}} \left(\sqrt{T} \beta^* \right)^B \left(\sqrt{1-T} \beta^* \right)^M \left(\frac{T}{(1-T)\beta^*} \right)^n \\ &\quad \times \sum_{k=\max(0, n-M)}^{\min(n, B)} \binom{M}{n-k} \binom{B}{k} \left(-\frac{1-T}{T} \right)^k, \end{aligned} \quad (12)$$

where the summation over k indicates the splitting of the n th element between the modes A and B .

The photon number distribution P_N is given by the diagonal elements of the density matrix ρ_{NN} , obtained from Eq. (10). Considering for example the single photon Fock state $\hat{\rho}_a = |1\rangle \langle 1|$ we obtain

$$\begin{aligned} P_N^{(1)} &= \frac{1!}{N!} e^{-|\beta|^2} [(1-T)|\beta|^2]^N \frac{T}{(1-T)|\beta|^2} \\ &\quad \times \sum_B \frac{(T|\beta|^2)^B}{B!} \left[\sum_k \binom{N}{n-k} \binom{B}{k} \left(-\frac{1-T}{T} \right)^k \right]_{k=0,1}^2 \\ &= e^{-(1-T)|\beta|^2} \frac{[(1-T)|\beta|^2]^N}{N!} \left\{ (1-T) + \frac{T[N - (1-T)|\beta|^2]^2}{(1-T)|\beta|^2} \right\}, \end{aligned} \quad (13)$$

and the summation over B resembles the expansion of exponential function but multiplied by a second order polynomial with respect to B . Each term in the summation converges and turns into an exponential $e^{T|\beta|^2}$ times a Bell polynomial of the argument

$T|\beta|^2$. For the vacuum contribution, $N = 0$, the summation index k can only take the value 1, otherwise the accepted indices are $k = 0, 1$. If we choose $T = 0$ in Eq. (13), the whole signal gets reflected and the photon number distribution at the output arm results in Poissonian distribution. In case $T = 1$, the Fock state is transmitted through the beam splitter without any interference with the reference beam and will not be displaced at all. Then, the measured photon number distribution corresponds to the one of the single photon Fock state. In Sec. 4 we will consider the case of $T = 95\%$.

B) Lossy channel followed by ideal displacement

Let us compare the last result with a model that considers losses in front of an ideal displacement $\hat{D}(\alpha)$ as shown in Fig. 2b. In this case the quantum state interferes with vacuum at the beam splitter with transmittance T . The loss degraded density matrix is again evaluated using Eq. (7), where we consider the Fock state $|n\rangle$ at the input i.e. $\hat{\rho}_a = |n\rangle\langle n|$. Taking into account the loss, the m -th diagonal element of the density matrix can be written as

$$\rho_{mm} = \binom{n}{m} T^m (1-T)^{n-m}, \quad (14)$$

where n is the number of incident photons, m is the number of transmitted photons, and $n - m$ the number of lost photons. The loss degraded density matrix has the form $\hat{\rho}_L = \sum_m \rho_{mm} |m\rangle\langle m|$, which leads to the following photon number distribution

$$\begin{aligned} P_N^{\hat{D}|n\rangle} &= \text{Tr} \left\{ \hat{D}(\alpha) \hat{\rho}_L \hat{D}^\dagger(\alpha) |N\rangle\langle N| \right\} \\ &= \sum_m \rho_{mm} \left| \langle m | \hat{D}(\alpha) | N \rangle \right|^2. \end{aligned} \quad (15)$$

It can be shown that the above matrix elements result in Laguerre polynomials [23]. Considering the single photon Fock state, the photon number statistics can be expressed as

$$\begin{aligned} P_N^{\hat{D}|1\rangle} &= (1-T) \left| \langle 0 | \hat{D}(\alpha) | N \rangle \right|^2 + T \left| \langle 1 | \hat{D}(\alpha) | N \rangle \right|^2 \\ &= e^{-|\alpha|^2} \frac{|\alpha|^{2N}}{N!} \left[1 - T + \frac{T(N - |\alpha|^2)^2}{|\alpha|^2} \right], \end{aligned} \quad (16)$$

which coincides with Eq. (13) when the displacement is $\alpha = \sqrt{1-T} \beta$. We can conclude that the action of the non-ideal displacement on the single photon Fock state corresponds actually to a loss applied before an ideal displacement, and a lower transmittance parameter T can be exchanged against the presence of higher loss.

In the next section the theory is extended to include the description of a non-ideal photon number resolving detector, which will be used in our simulations.

3. Loss tolerant characterisation using TMD

In order to gain information about the Wigner function of an incoming state applying the sampling technique we can use an experimental setup as shown in Fig. 3. The quantum

signal is superimposed with a reference beam on a high-transmission beam splitter, such that it gets displaced in phase space. While the reflected signal beam is neglected, the transmitted one is launched into a time multiplexing detector (TMD), for measuring the displaced photon number distribution. Photon counting is accomplished in a TMD by distributing one multi-photon-event in different modes, which are analysed with binary detectors. The TMD consists of a beam splitter network and has a fibre integrated implementation with fibre loops of variable lengths, such that a pulse launched into the detector is divided into a train of pulses via several 50/50 beam splitters couplers [17, 18]. The existence of photons in each mode (or time-bin) can be detected by APDs. From the measured data the so-called click-statistics are collected, which record the number of bins containing a detection event.

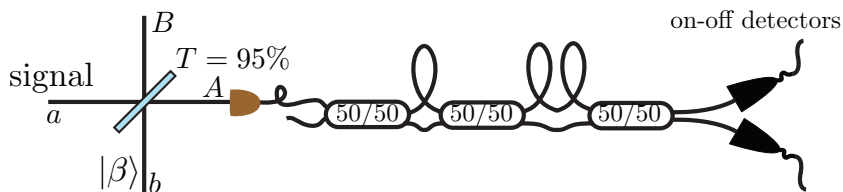


Figure 3. Experimental scheme for sampling the Wigner function. The quantum signal is displaced with a weak reference beam in a high-transmission beam splitter and is then launched into TMD, enabling to resolve the number of photons.

Using the TMD, the measured click statistics $\vec{p} = (p_0, p_1, \dots, p_n)$ is related to the input photon number distribution $\vec{\rho} = (\rho_{00}, \rho_{11}, \dots, \rho_{nn})$ through the relation [24]

$$\vec{p} = \mathbf{C} \mathbf{L}(\eta) \vec{\rho}. \quad (17)$$

The convolution matrix \mathbf{C} takes into account the stochastic distribution of n photons into several bins (from which follows that the number of clicks m is lower or equal to n) and the matrix $\mathbf{L}(\eta)$ describes the binomial process of loss,

$$L_{m,n} = \begin{cases} \binom{n}{m} \eta^m (1-\eta)^{n-m}, & \text{when } m \leq n \\ 0 & \text{otherwise.} \end{cases} \quad (18)$$

Therefore, by inverting equation (17) or using a maximum likelihood technique, the photon number distribution of the quantum signal can be reconstructed from the click statistics if the loss η and the convolution matrix are known. Beside the numerical techniques an analytical solution presented in Appendix A can be used for inverting the losses.

In previous work [11], the analysis of the sampling method was done considering a network with a high-transmission beam splitter followed by a loss element and an ideal photon counter. In our analysis we want to elaborate how we can use a TMD as photon counter in conjunction with loss-tolerant characterisation for determining the displaced photon statistics and the Wigner function. For this we need to modify the

detection model such that the order of the beam splitters modelling the losses and the displacement are interchanged. Combining all losses together (treating them as one overall loss η_2) and moving them in front of the displacement enables us to invert the click statistics of the displaced quantum states [Eq. (17)], i.e. we can study the displaced statistics independent from detector inefficiencies.

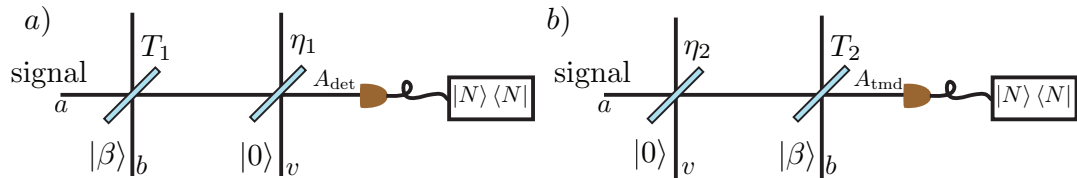


Figure 4. Two possible networks for modelling the displacement and loss degradation of the quantum state: (a) intuitive model, where the detection losses are after the displacement, (b) model used in TMD analysis, where all the losses are brought in front of the beam splitter network enabling the loss inversion.

The corresponding schemes are shown in Fig. 4, and we can compare them by calculating the evolution of the annihilation operators through the networks. The creation operator of the model in Fig. 4a obeys Eq. (6) with $T = T_1$ and $\eta = \eta_1$. Similar transformation for the model in Fig. 4b gives

$$\begin{aligned} \hat{A}_{\text{TMD}} &= \sqrt{\eta_2 T_2} \hat{a} + \sqrt{1 - T_2} \hat{b} + \sqrt{T_2(1 - \eta_2)} \hat{v} \\ &= \sqrt{\eta_2 T_2} \left(\hat{a} + \sqrt{(1 - T_2)/\eta_2 T_2} \hat{b} \right) + \sqrt{T_2(1 - \eta_2)} \hat{v}. \end{aligned} \quad (19)$$

According to Eqs. (6) and (19) the efficiencies of the networks are $\eta_1 T_1$ and $\eta_2 T_2$, and the displacement set by the reference beam is modified by factors $\sqrt{\frac{1 - T_1}{T_1}}$ and $\sqrt{\frac{1 - T_2}{\eta_2 T_2}}$ for the models in Figs. 4a and 4b respectively. If the following criteria

$$\begin{aligned} T_2 &= (1 - \eta_1) + \eta_1 T_1 \quad \text{and} \\ \eta_2 &= \frac{\eta_1 T_1}{T_2} \end{aligned} \quad (20)$$

are fulfilled, the annihilation operators at the output ports of the networks are equivalent and the two situations can not be distinguished.

Thus, although the model in Fig. 4a presents an intuitive description of the physical process of displacing a state and measuring it with non-ideal quantum efficiency, the model in Fig. 4b gives mathematically the same result. The appropriate pair of parameters T_2 and η_2 are derived from the values of T_1 and η_1 , which can be precisely calibrated using properties of PDC twin-photons [19, 20].

4. Monte Carlo Simulations

In the experiment the quantum state of interest is prepared several times enabling the realisation of an ensemble measurement, which allows the reconstruction of the photon number statistics. Here, a similar scenario is achieved using a Monte Carlo simulation.

The photon number statistics of the displaced Fock state can be evaluated with the help of Eq. (10). The same equation can be employed to calculate the effect of loss if the reference beam $|\beta\rangle$ is replaced by vacuum. We performed a simulation to generate the statistics of the quantum state and convoluted it with the known stochastic description of the TMD, thus simulating the detected photon number distribution. In order to estimate the statistical errors, we performed for each sampled point of the phase space ten different Monte Carlo simulations, each consisting of 10^6 events. The chosen number of events is based on the number of expected experimental realisations, which depends, e.g., on the setup stability.

We performed two different types of simulations considering the Fock states $|1\rangle$ and $|2\rangle$ as input signals. As these states are symmetric in phase space, we assumed a fixed value for the relative phase between signal and reference beam, changing only the amplitude of the displacement. We studied a certain range in the phase space and restrict the coherent reference beam to have maximally the mean photon number of $\langle n_\beta \rangle \sim 49$. Thus, we set the upper limit of the summation in Eq. (10) to 100 in order to avoid numerical errors.

To recover the photon number statistics of the displaced state we employed the direct numerical inversion of Eq. (17), which together with Eq. (2) yields the reconstructed Wigner function. There are two factors limiting the range for a reliable reconstruction. First, as a consequence of the TMD resolution, the mean photon number of the displaced beam is restricted. With a m -stage TMD, i.e. the number of 50/50 couplers, we are in principle able to resolve maximally upto 2^m clicks. For example, in the case of a 3-stage (8-bin) TMD, we note that errors begin to accumulate if the probability of having more than 8 photons in the displaced signal is on the order of 2-3%. The second limitation arises from statistical errors and can be estimated from the amount of events collected versus losses. Statistical errors are highly amplified in the loss inversion process. As the losses increase the inversion becomes unstable, i.e. the loss matrix becomes singular entailing negative probability components for the reconstructed photon number statistics. In this case the negative components are due to high-photon number contributions. We define the reliable reconstruction range by a boundary value for the displacement, at which the inversion becomes unstable or, similarly, the photon number statistics reconstructed from the 10 simulations render negative probability components larger than 0.1%.

Experimentally, losses are considerably high. For example, APDs have quantum efficiencies as low as 60-80% at 800nm. The coupling efficiency into single-mode fibres is highly mode sensitive and can drop down to 30-40% for mismatched modes. Effectively, a realistically achievable detection efficiency for a state characterisation setup lies between 20-30%. Additionally, losses due to other optical components may also not be negligible. An important source causing degradation of the signal is the beam splitter used as displacement element. Typically, the transmittance of the displacement beam splitter is around a value of 95%. Due to the 5% reflectance, the beam splitter intrinsically attenuates the quantum signal and modifies the displacement. In addition

to the effect caused by inefficiencies or losses, we must take into account the accuracy at which the convolution matrix of the TMD can be determined. A non-uniform bin probability distribution is due to unbalanced 50/50 couplers, which are generally specified with 5% uncertainty.

Beyond the investigation of reconstructing the Wigner functions our simulations also allows us to directly explore the non-trivial photon number distributions of displaced Fock states. Presenting an exact photon number, Fock states exhibit a completely undetermined phase, which can be depicted by a rotational symmetry of the field's quadratures around the origin of the phase space. In other words, Fock states can be imagined as rings around the origin (uncertain phase) that have definite amplitudes (exact photon numbers). Detecting photon statistics corresponds to evaluating the overlap of the studied signal state with Fock states. Using this concept it becomes intuitive that the photon number distributions of displaced Fock states must present oscillations, as a consequence of the interference in the phase space [25, 26, 27]. These oscillations are presented in Fig. 5 for the states $|1\rangle$ and $|2\rangle$. We clearly see that displacing, e.g., the single photon Fock state, the probability of measuring one photon starts to decrease and is finally maximally suppressed when the displacement reaches the mean photon number $\langle n_\alpha \rangle = 1$. In Sec. 5 this quantum behaviour is explored in order to discern the effects of losses from imperfect mode overlap between signal and reference beam.

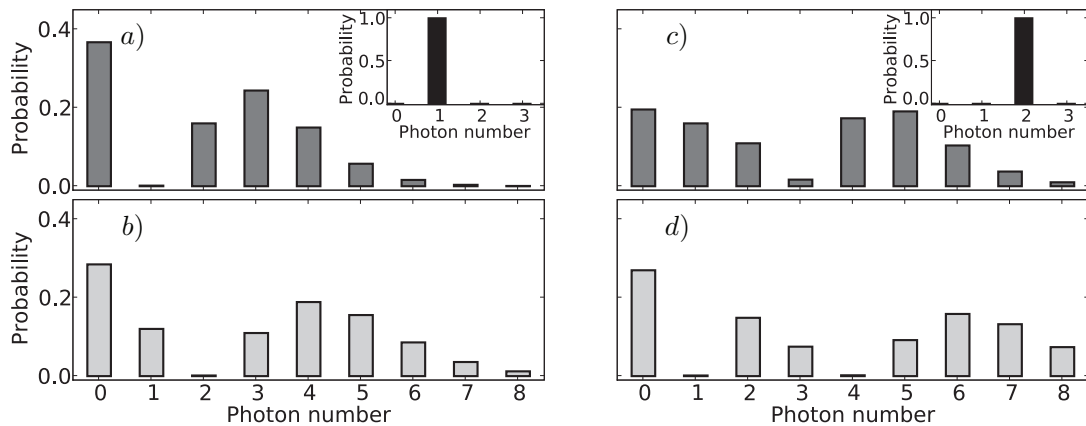


Figure 5. Photon number distribution for displaced a-b) single and c-d) two photon Fock states. The distributions are presented at two values of displacement: $\alpha = 1.0$ (dark grey) and $\alpha = 1.4 \sim \sqrt{2}$ (light grey). The insets show the photon number distributions at $\alpha = 0$.

4.1. Results

We performed the simulation for three different scenarios to clarify which kind of effects each experimental frame gives. We analysed the performance of the state characterisation and estimated the limitations by considering a realisable displacement

operator implemented with a beam splitter of 95% transmittance, by assuming 8-bin and 16-bin TMDs and including the convolution matrices, and further by taking into account a finite detection efficiency.

Case 1: First we studied the effect of displacing the signal via a beam splitter with 95% transmittance. The simulations were performed assuming ideal detection efficiency and uniform distribution of photons on a 8-bin TMD. The reconstructed Wigner functions for Fock states $|1\rangle$ and $|2\rangle$ are slightly loss degraded due to the beam splitter, but this degradation can easily be handled with the direct inversion as shown in Fig. 6. With lossless detection, the 8-bin TMD is adequate to scan the interesting regions of the phase space for both of these states. Due to the limited number of TMD stages, a reliable reconstruction of $W(\alpha)$ is possible only inside a given scanning range of phase space, i.e. there is a maximum value of α that can be safely applied. Therefore, the ultimate boundaries for the reliable scanning ranges correspond to displacements of $\alpha = 1.5$ and $\alpha = 1.2$ for states $|1\rangle$ and $|2\rangle$, respectively.

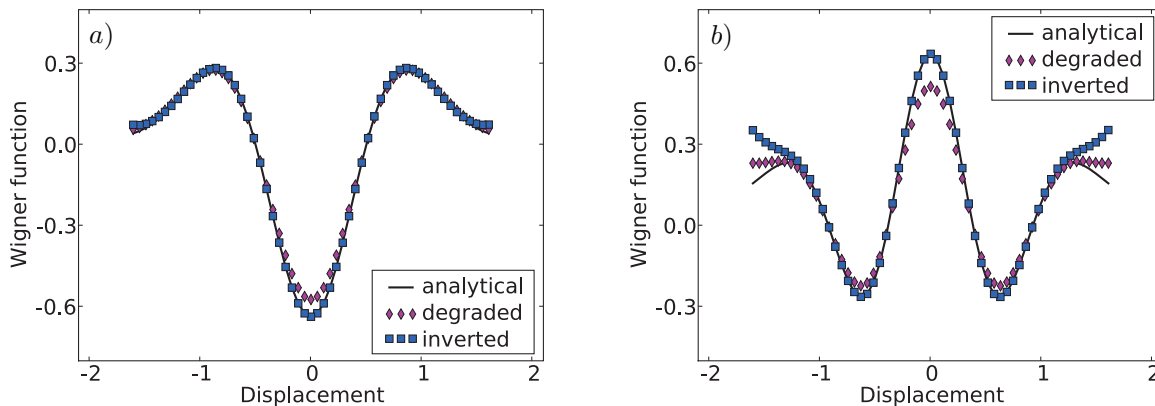


Figure 6. Loss degraded (diamonds), reconstructed (squares), and analytical (solid line) Wigner functions for Fock states a) $|1\rangle$ and b) $|2\rangle$. The simulated setup has a displacing beam splitter with 95% transmittivity and ideal detection efficiency. The reconstruction is very accurate with errors smaller than used symbols. For further details see text.

Case 2: In the second simulation we considered more realistic parameters, which might be accessible in the near future. We assumed a detection efficiency of 60% as well as an unbalanced TMD bin distribution, with splitting ratios of 45/55. The deconvolution however was still done by assuming the couplers to have 50/50 ratios. Fig. 7 shows a comparison between the reconstruction of single photon Fock state with 8-bin and 16-bin TMDs. As the detection efficiency decreases, the effect of the loss becomes prominent restricting the reliable scanning range in the phase space. Note that the 16-bin TMD does not perform much better than the 8-bin TMD. The direct inversion of the Fock state $|1\rangle$ breaks down for the 8-bin TMD close to a displacement of 1.2, while in the

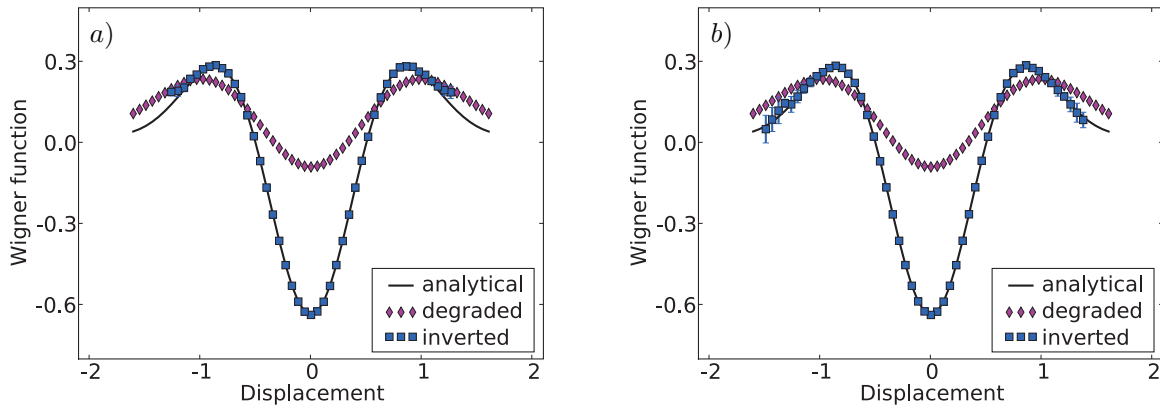


Figure 7. Loss degraded (diamonds), reconstructed (squares), and analytical (solid line) Wigner functions for the single Fock state $|1\rangle$. a) 8-bin and b) 16-bin TMDs were analysed in a setup of 60% detection efficiency. No apparent error bars means that the errors are smaller than used symbols.

case of the 16-bin TMD the state reconstruction range is reliable up to a displacement of 1.4.

Case 3: The third simulation resembles a scenario of a currently feasible experimental situation with a detection efficiency of 30%. Again, we assumed an unbalanced TMD with coupling ratios of 45/55 and balanced deconvolution. In this high loss regime there is basically no difference between the 8-bin and 16-bin TMDs. As shown in Fig. 8 the loss has shrunk the reliable reconstruction ranges from the earlier cases. The negative parts of the loss degraded Wigner functions are completely washed out. Nevertheless, the inner regions of the Wigner functions can still be reliably reconstructed up to displacements of 0.8 and 0.6 for the states $|1\rangle$ and $|2\rangle$, respectively. The inversion causes negative components also near the zero displacement for the Fock state $|2\rangle$ indicating that the inversion is unstable. This is not caused by the contribution of higher photon numbers but by the accuracy at which vacuum, one and two photon components are recorded. We accept the results at these displacements as the error in the parity measurement is negligible.

Despite the low efficiency (30%), the simulation indicates that we are able to reconstruct the oscillatory behaviour of the photon number statistics for the Fock states $|1\rangle$ and $|2\rangle$. In Fig. 9 we show the loss degraded, inverted and expected photon statistics when no displacement is applied and when the highest reliable displacement is applied to the quantum signal state. The loss obscures the oscillations of the photon statistics, but similarly to the Wigner function analysis, using the inversion technique we are able to reconstruct this behaviour from the TMD measurement.

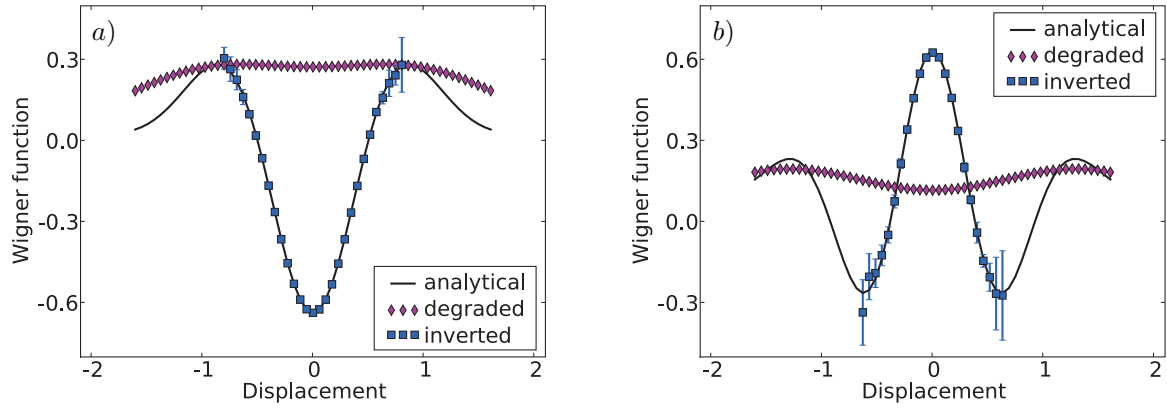


Figure 8. Loss degraded (diamonds), reconstructed (squares), and analytical (solid line) Wigner functions for Fock states a) $|1\rangle$ and b) $|2\rangle$. In both simulations 8-bin TMDs were considered in conjunction with 30% detection efficiency.

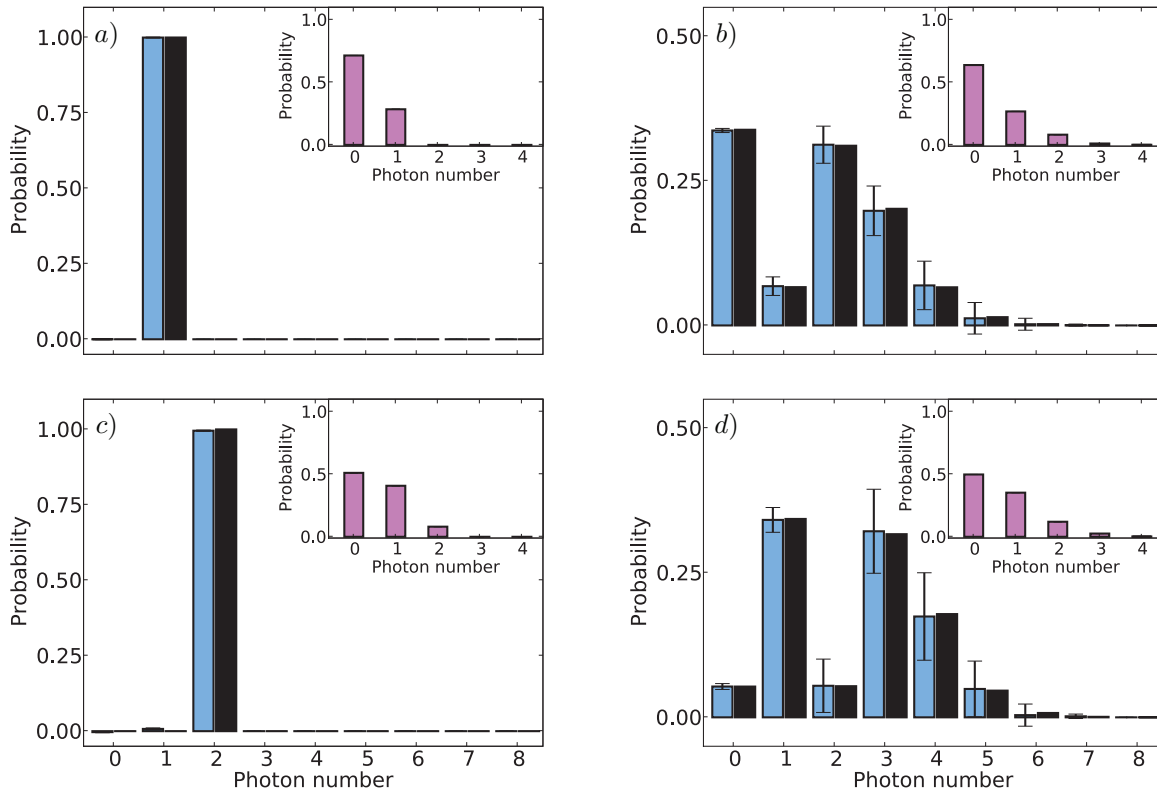


Figure 9. Simulated statistics at the values of a) $\alpha = 0$ and b) $\alpha = 0.8$ for the single photon Fock state and at c) $\alpha = 0$ and d) $\alpha = 0.6$ for the two photon Fock state. The loss degraded (pink, inset) and inverted (blue) statistics are shown together with the analytical solution of the photon number distribution (black). The two extreme cases of no displacement (left side) and the highest displacement (right side) allows a reliable state reconstruction despite of the low detection efficiency – 30%.

5. Imperfect mode overlap between quantum signal and reference beam

Mode overlap is a crucial issue for both unbalanced and balanced characterisation techniques. In balanced homodyne measurements imperfect mode overlap has the same signature as loss, since only the overlapping part of signal state contributes to the detected photo currents. Contrariwise, in unbalanced measurements, as the sampling technique, all photons impinging on the photon counter are detected, and an imperfect mode overlap results in a convolution of several photon number distributions.

We model the imperfect mode overlap by the beam splitter network shown in Fig. 10. The signal and the reference beam are divided into four modes, from which only two interfere. The part of the quantum signal that does not overlap with the reference beam is reflected by a beam splitter with transmittance t_1 into an ancillary mode. Accordingly, the part of the reference beam that does not overlap with the signal is reflected into another mode at a beam splitter with transmittance t_2 . The degree of overlap is chosen via the parameters t_1 and t_2 , whose square is interpreted as the percentage of the signal state and of the reference beam that interferes.

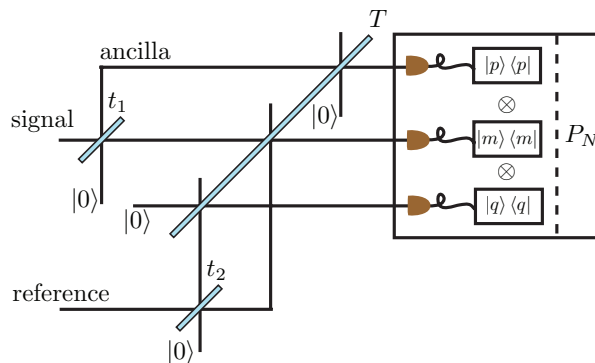


Figure 10. Model for imperfect mode overlap. The signal and the coherent reference beam are divided into four modes in two different beam splitters, with transmittances t_1 and t_2 , respectively. In this scheme, m corresponds to the number of detected overlapped photons, while the number of not overlapping photons p or q is arising from the ancillary mode or from the uncorrelated reference beam, respectively.

We are interested in the joint probability distribution $P(m, p, q)$ for the three detection arms of the network, where m corresponds to the number of overlapped photons, p to the number of non-overlapping photons arising from quantum signal state, and q to the number of non-overlapping photons coming from the reflected coherent reference beam. As the coherent reference beam is divided into two uncorrelated parts we assume a joint probability distribution composed of two independent probability distributions, $P(m, p, q) = P(p, m)P(q)$. The detected photon number distribution is then given as the convolution of the distributions in the three detection arms,

$$P_N = \sum_{N=p+m+q} P(m, p)P(q). \quad (21)$$

With Eq. (21) we can now calculate the photon number distribution for Fock states in the presence of mode mismatch between the reference and the signal state. The Fock state $|n\rangle = \frac{1}{\sqrt{n!}}(\hat{a}_{in}^\dagger)^n |0\rangle$ is launched into the first beam splitter with transmittance t_1 interfering with the vacuum coming from the other input arm. The state is divided into the signal (s) and ancillary (a) modes by

$$|\varphi\rangle_{s,a} = \sum_{k=0}^n \sqrt{\binom{n}{k}} \sqrt{t_1^{n-k} (-\sqrt{1-t_1})^k} |n-k\rangle_s |k\rangle_a, \quad (22)$$

where we have used the beam splitter transformation $\hat{\mathcal{U}}$ from Eq. (5) and the binomial expansion. The density matrix of the two mode state $|\varphi\rangle_{s,a}$ has the form

$$\rho = \sum_{k,l} \sqrt{\binom{n}{k} \binom{n}{l}} \sqrt{t_1^{2n-k-l} (-\sqrt{1-t_1})^{k+l}} |n-l\rangle_s \langle n-k| \otimes |l\rangle_a \langle k|. \quad (23)$$

This state is thereafter sent through the displacing beam splitter (transmittance T), upon which the signal mode interferes with the overlapping coherent state $|\gamma\rangle$, whereas the ancillary mode gets combined with vacuum. The joint probability distribution $P(m, p)$ of detecting m -photons in the signal arm and p -photons in ancillary arm is then given by

$$P(m, p) = \sum_{k,l} \sqrt{\binom{n}{k} \binom{n}{l}} \sqrt{t_1^{2n-k-l} (-\sqrt{1-t_1})^{k+l}} P_a(p) P_s(m), \quad (24)$$

with $P_a(p)$ and $P_s(m)$ denoting the probability distributions for the detectors at the ancillary and signal arms respectively. These can be evaluated with the help of Eqs. (8)–(12). Considering the ancillary mode, we can make the following substitutions in Eq. (8): $\hat{\rho}_a \rightarrow |l\rangle_a \langle k|$ and $|\beta\rangle_b \rightarrow |0\rangle$, which yields the photon number distribution of the ancillary arm

$$P_a(p) = \binom{l}{l-p} T^p (1-T)^{l-p} \delta_{k,l}. \quad (25)$$

The Kroenecker delta-function $\delta_{l,k}$ arises due the fact that only the contributions from the diagonal terms of the density matrix contribute to the detection. The form of the joint probability distribution in Eq. (24) simplifies to

$$P(m, p) = \sum_{l=0}^n \binom{n}{l} t_1^{n-l} (1-t_1)^l \binom{l}{l-p} T^p (1-T)^{l-p} P_s^{\delta_{k,l}}(m), \quad (26)$$

where $P_s^{\delta_{k,l}}(m)$ is the probability distribution of the displaced signal. This distribution can again be evaluated with the help of Eq. (8), now making the substitutions: $\hat{\rho}_a \rightarrow |n-l\rangle_a \langle n-l|$ and $|\beta\rangle_b \rightarrow |\gamma\rangle$.

The effective reference beam $|\gamma\rangle$ that overlaps with the quantum signal is given by the transmission of the initial coherent field $|\beta\rangle$, i.e. $|\gamma\rangle = |\sqrt{t_2}\beta\rangle$. In the same way, the

non-overlapping part has the form $|\sqrt{1-t_2}\beta\rangle$. The last one results in an independent Poissonian distribution at the detection, given by

$$P(q) = \frac{[(1-T)(1-t_2)|\beta|^2]^q}{q!} e^{-(1-T)(1-t_2)|\beta|^2}. \quad (27)$$

We performed Monte Carlo simulation to study the effect of imperfect mode overlap on the single photon Fock state according to Eq. (21), (26) and (27). We generated the distribution P_N again ten times, each consisting of 10^6 events, enabling us to construct the photon number statistics and to estimate the error (similar to simulation presented in Sec. 4). Further we utilise a beam splitter with 95% transmittance for the overlap and an 8-bin TMD with uniform bin distributions.

First we studied the differences between ideal ($t_1 = t_2 = 1$) and non-existing ($t_1 = t_2 = 0$) mode overlaps. The statistics is reconstructed by inverting with 95% efficiency, which corresponds to the intrinsic loss introduced by the displacement beam splitter. In Figs. 11a and 11c we show the characteristic behaviour of the vacuum P_0 and one photon P_1 components of the statistics for the both cases. Remember from our discussion about the oscillating photon statistics in Sec. 4 that in case of the ideal overlap we expect a suppression in the one photon component P_1 when the displacement is equal to one. As expected this behaviour is recovered in our simulation as seen in Fig. 11a. Contrarily in the non-overlapping case (Fig. 11c), the statistics is given by a convolution of single photon state $|1\rangle$ and coherent field $|\beta\rangle$, which has a different mean photon number for each value of displacement. Thus, an increment in the displacement decreases the one photon component, nevertheless the characteristic oscillation of P_1 is no longer observable. This Gaussian behaviour of P_1 is caused by the Poissonian vacuum component of the reference beam. Another clear signature of a lack of mode match is seen in the vacuum component of the inverted statistics: in the case of no overlap this contribution is always zero independent of the displacement. This effect is opposed to the one caused by losses, that always increases the probability of lower photon numbers.

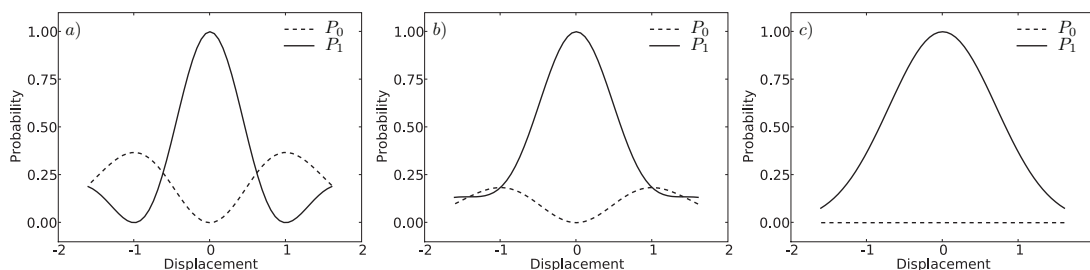


Figure 11. The behaviour of the vacuum and one photon components of the statistics vs. the displacement of the single photon Fock state in the cases of a) perfect overlap ($t_1 = t_2 = 1$), b) 50% overlap ($t_1 = 0.5, t_2 = 1$) and c) no overlap ($t_1 = t_2 = 0$).

Next we consider an intermediate case, assuming 50% of overlap between the single photon Fock state and the reference beam ($t_1 = 0.5, t_2 = 1$). Because of the imperfect

overlap the amplitude of the photon number oscillation is reduced, but still visible. Nevertheless, the analysis of Figs. 11b and 12a-b shows the characteristic behaviour of an mode mismatch: slow increment of P_0 and lack of suppression of P_1 , as the displacement is increased. This simple feature provides a route for evaluating the degree of overlap. In addition, the width of the reconstructed Wigner function becomes broader, when compared to the analytical solution (Fig. 12c). Further, the positive tips seen on the wings cannot be properly reconstructed because the one photon contribution is not totally suppressed.

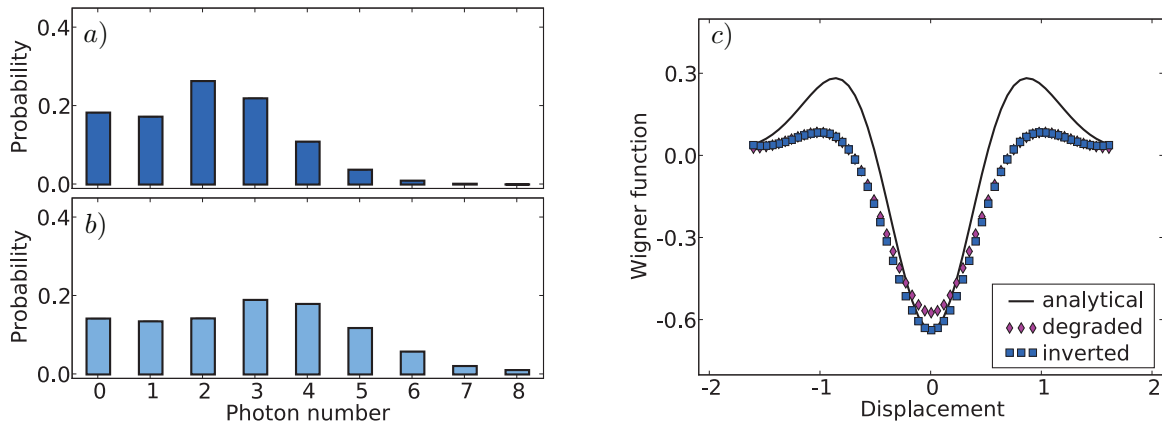


Figure 12. Statistics of the single photon Fock state at displacements a) 1.0 and b) 1.4 together c) the Wigner function considering 50% overlap. The reconstructed Wigner function (diamonds) presents a broader width, which is a clear signature of imperfect overlap.

Finally, we combine the effect of losses with imperfect overlap. We assume that the single photon Fock state has been affected by loss (detection efficiency equal to 30%) before applying a non-ideal displacement ($t_1 = 0.5, t_2 = 1$). In Fig. 13 we show the photon number statistics for both the degraded and reconstructed signals at different values of the displacement. The quantum feature of photon number oscillation is washed out by losses as well by imperfect overlap. Nevertheless, the first effect can still be handled by applying an appropriate inversion method, which emphasises the importance of the beam-splitter network model applied in this work (Fig.4b). The reconstructed photon number statistics and thus the Wigner function are equal to the one obtained in last case (ideal detection efficiency, Fig.12), except from the fact that the reliable maximal displacement is now restricted, due to instabilities caused by the losses. We employed a limit to the reliable displacement range defined by the occurrence of negative probability larger than 0.3%. In terms of displacement this limit is equal to 1.0, being the boundary value for the reconstruction of the the Wigner function. As shown in Fig. 14, the Wigner function determined via the degraded signal does not display any quantum features. However, using the inversion of the statistics, the negative inner parts are recovered, although with a broadened width as a consequence of the imperfect mode overlap.

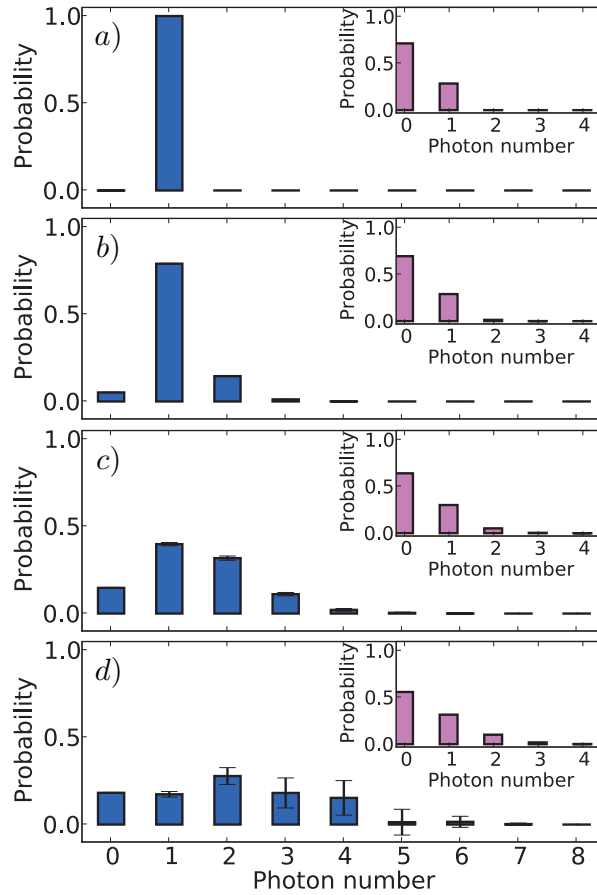


Figure 13. The loss degraded (inset) and reconstructed photon number statistics of the single photon Fock state. The state is affected by loss ($\eta = 30\%$) before the displacement with 50% overlap. The following values of displacement were applied a) 0, b) 0.3, c) 0.7, d) 1.0.

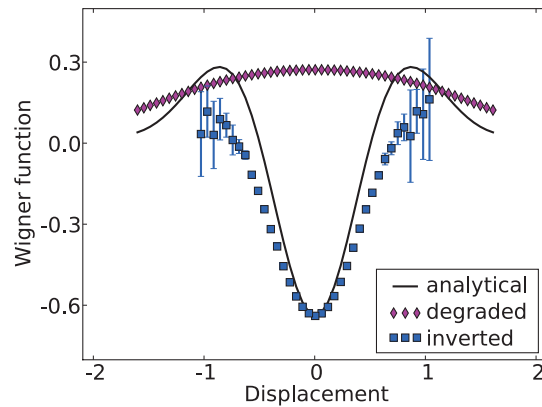


Figure 14. Loss degraded (diamonds), reconstructed (squares), and analytical (solid line) Wigner functions for the single photon Fock state using the inverted statistics of Fig. 13.

A further analysis using this model will consider a thorough investigation of the convolution effects in Eq. (21), such that the exact degree of overlap could be reliably extracted from the detected click statistics. Despite of the fact that an analytical solution to this question is not given, the presented analysis provides, to our knowledge for the first time, qualitative features that discern the effect of losses from imperfect overlap. By fitting this model to the experimental data, the value of the degree of overlap can be extracted.

6. Conclusions

We studied the ability to reconstruct the Wigner function of low-photon-number Fock states in a TMD based photon counting experiment. This kind of experiment offers the opportunity of loss-tolerant characterisation via the inversion of losses, and enables to probe the Wigner function point by point in the phase space.

We calculated the photon number distribution after displacing the state with an asymmetric beam splitter, showing that this setup can be efficiently modelled by a loss element in front of an ideal displacement for a single photon Fock state. Several parameters restrict the reliable reconstruction range in phase space: the number of TMD bins with respect to the mean photon number of the studied quantum state, the stability of the inversion and the loss level. With current technology, the detector efficiency level is the dominant limitation.

Performing Monte Carlo simulations we reconstructed the Wigner functions for single and two photon Fock states at different levels of detection efficiency. The photon number distributions of displaced Fock states present a characteristic oscillatory behaviour that, in the low efficiency level, are washed out. Nevertheless, the oscillatory feature can be reliably restored through the loss-inversion. A clear indication of phase space interference is given by the suppression of the one-photon component after displacing the single photon Fock state. The presented simulations show that for perfect mode-matching the Wigner function of single photon Fock state can be reconstructed with high confidence.

Finally, we presented a model allowing to estimate the degree of mode overlap between the quantum signal and the reference beam, used for realising the signal's displacement. The model is based on a simple beam splitter network, where the information carried by the overlapping and non-overlapping parts give rise to a joint probability distribution. By performing a Monte Carlo simulation we studied the reconstruction of the characteristics of the single photon Fock state. A lack of mode matching is recognised from an exponential decrease in the one photon component as the displacement is increased. Also, contrarily to losses, an absence of overlap decreases the expected vacuum components in the statistics of the displaced single photon Fock state. Even in a scenario of 50% overlap the reconstructed Wigner function shows negative values, although with a broader width.

Our results motivate the experimental exploration of non-Gaussian states with

photon number resolving detectors, even in the situation of rather low detection efficiencies. Furthermore, the sampling method allows an advanced quantum state characterisation that is intrinsically not only sensitive to a single mode but takes into account all characteristics of the original quantum state and the coherent reference beam. In our paper, we provided the tools to reliably characterise the prepared state and highlighted the different impacts of inefficient detection, convolution of statistics and mode mismatch. In contrast to usual homodyne detection, our analysis enables us to recognise the type of experimental imperfections, and gives valuable information about the extent of degradation caused by each one. Thus, our work constitutes a basis for a broad understanding of experimental data. We expect that our investigation opens a new route of detecting and studying quantum states and offers a new experimental technique for both CV and discrete variable based quantum information applications.

Acknowledgments

We would like to acknowledge fruitful discussions with T. C. Ralph, W. Schleich and W. Vogel. This work was supported by the EU under QAP funded by the IST directorate as Contract No. 015848.

Appendix A. Derivation of the Wigner function from loss degraded statistics

In this section we derive an analytical solution for constructing the Wigner function from the loss degraded statistics. The elements of the loss matrix are determined by the Eq. (18), and the loss degraded statistics p_m^L is connected to the photon number statistics by

$$p_m^L = \sum_{n=0}^N \binom{n}{m} \eta^m (1-\eta)^{n-m} \rho_{nn}, \quad (\text{A.1})$$

where N is the highest resolvable photon number at detection, m is the amount of detected photons while n is the amount of incident photons. In the low-loss regime the direct inversion of the loss matrix is possible by

$$L_{m,n}^{-1} = \begin{cases} \binom{n}{m} \frac{(-1+\eta)^{n-m}}{\eta^n}, & \text{when } m \leq n \\ 0 & \text{otherwise,} \end{cases} \quad (\text{A.2})$$

where n now corresponds to the number of loss degraded detection events and m is the number of photons in the signal state. Note that both matrices in Eqs. (18) and (A.2) are upper diagonal matrices.

The inverted photon number statistics is given by

$$\rho_{mm} = \sum_{n=0}^N \binom{n}{m} \frac{(-1+\eta)^{n-m}}{\eta^n} p_n^L. \quad (\text{A.3})$$

The reconstruction of the photon number m is affected by all lower photon numbers satisfying $n \geq m$. The expression for the Wigner function in Eq. (2) can be evaluated using the degraded statistics in Eq. (A.3)

$$\begin{aligned}
W &= \frac{2}{\pi} \sum_{m=0}^N (-1)^m \rho_{mm} \\
&= \frac{2}{\pi} \sum_{n=0}^N \frac{1}{\eta^n} \left[\sum_{m=0}^n \binom{n}{m} (-1 + \eta)^{n-m} (-1)^m \right] p_m^L, \quad m \leq n \leq N \\
&= \frac{2}{\pi} \sum_{n=0}^N \left(-\frac{2-\eta}{\eta} \right)^n p_n^L. \tag{A.4}
\end{aligned}$$

The result of Eq. (A.4) coincides with the independent analysis presented in Ref. [11] and corresponds to scaling of the parity factor by the detection efficiency.

We can apply this method for example on the loss degraded statistics of the single photon Fock state derived in Eq. (16). The loss inverted Wigner function can be written as

$$\begin{aligned}
W &= \frac{2}{\pi} \sum_M^{N \rightarrow \infty} \left(-\frac{2-T}{T} \right)^M e^{-|\alpha|^2} \frac{|\alpha|^{2M}}{M!} \left[1 - T + \frac{T(M - |\alpha|^2)^2}{|\alpha|^2} \right] \\
&= \frac{2}{\pi} e^{-2\frac{|\alpha|^2}{T}} \left[4\frac{|\alpha|^2}{T} - 1 \right]. \tag{A.5}
\end{aligned}$$

In the limit of $N \rightarrow \infty$ (no restriction set by maximum resolvable photon number), the summation in Eq. (A.5) can be evaluated. If we further set $\alpha = \sqrt{1-T}\beta$, the reconstructed Wigner function corresponds to the one of the single Fock state displaced by $\sqrt{\frac{1-T}{T}}\beta$.

References

- [1] J. Eisert, S. Scheel, and M. B. Plenio. Distilling gaussian states with gaussian operations is impossible. *Phys. Rev. Lett.*, 89(13):137903, 2002.
- [2] G. Giedke and J. I. Cirac. Characterization of gaussian operations and distillation of gaussian states. *Phys. Rev. A*, 66(3):032316, 2002.
- [3] A. I. Lvovsky, H. Hansen, T. Aichele, O. Benson, J. Mlynck, and S. Schiller. Quantum state reconstruction of the single-photon fock-state. *Phys. Rev. Lett.*, 87(5):050402, 2001.
- [4] K. Wakui, H. Takahashi, A. Furusawa, and M. Sasaki. Controllable generation of highly nonclassical states from nearly pure squeezed vacua. *Opt. Express*, 15:3568, 2007.
- [5] A. Ourjoumtsev, R. Tualle-Brouri, and P. Grangier. Quantum homodyne tomography of a two-photon fock-state. *Phys. Rev. Lett.*, 96:213601, June 2006.
- [6] A. Zavatta, V. Parigi, and M. Bellini. Toward quantum frequency combs: Boosting the generation of highly nonclassical light states by cavity-enhanced parametric down-conversion at high repetition rates. *Phys. Rev. A*, 78:033809, 2008.
- [7] K. Vogel and H. Risken. Determination of quasiprobability distributions in terms of probability distributions for the rotated quadrature phase. *Phys. Rev. A*, 40(5):2847, 1989.
- [8] D. T. Smithey, M. Beck, M. G. Raymer, and A. Faridani. Measurement of the wigner distribution and the density matrix of a light mode using optical homodyne tomography: application to squeezed states and the vacuum. *Phys. Rev. Lett.*, 70(9):1244, 1993.

- [9] A. I. Lvovsky and M. G. Raymer. Continuous-variable optical quantum state tomography. *arXiv:quant-ph/0511044*, 2005.
- [10] K. E. Cahill and R. J. Glauber. Density operators and quasiprobability distributions. *Phys. Rev.*, 177(5):1882, 1969.
- [11] S. Wallentowitz and W. Vogel. Unbalanced homodyning for quantum state measurements. *Phys. Rev. A*, 53(6):4528, 1996.
- [12] K. Banaszek and K. Wodkiewicz. Direct probing of quantum phase space by photon counting. *Phys. Rev. Lett.*, 76(23):4344, 1996.
- [13] K. Banaszek, C. Radzewicz, and K. Wodkiewicz. Direct measurement of the wigner function by photon counting. *Phys. Rev. A*, 60(1):674, 1999.
- [14] L. G. Lutterbach and L. Davidovich. Method for direct measurement of the wigner function in cavity qed and ion traps. *Phys. Rev. Lett.*, 78(13):2547, 1997.
- [15] P. Bertet, A. Auffeves, P. Maioli, T. Meunier, M. Brune, J. M. Raimond, and S. Haroche. Direct measurement of the wigner function of a one-photon fock state in a cavity. *Phys. Rev. Lett.*, 89(20):200402, 2002.
- [16] Ch. Silberhorn. Detecting quantum light. *Cont. Phys.*, 48(3):143, 2007.
- [17] M. J. Fitch, B. C. Jacobs, T. B. Pittman, and J. D. Franson. Photon number resolution using time-multiplexed single-photon detectors. *Phys. Rev. A*, 68(193):043814, 2003.
- [18] D. Achilles, Ch. Silberhorn, C. Sliwa, K. Banaszek, and I. A. Wamsley. Fiber-assisted detection with photon number resolution. *Opt. Lett.*, 28(23):2387, 2003.
- [19] D. Achilles, Ch. Silberhorn, and I. A. Wamsley. Direct, loss-tolerant characterization of nonclassical photon statistics. *Phys. Rev. Lett.*, 97(4):043602, 2005.
- [20] M. Avenhaus, H. B. Coldenstrodt-Ronge, K. Laiho, W. Mauerer, I. A. Wamsley, and Ch. Silberhorn. Photon number statistics of multimode parametric downconversion. *Phys. Rev. Lett.*, 101:053601, 2008.
- [21] K. Banaszek and K. Wodkiewicz. Accuracy of sampling quantum phase space in a photon counting experiment. *J. Mod. Opt.*, 44(11-12):2441, 1997.
- [22] M. G. A. Paris. Displacement operator by beam splitter. *Phys. Lett. A*, 217:78, 1996.
- [23] S. M. Barnett and P. M. Radmore. *Methods in theoretical quantum optics*. Oxford University Press, 1997.
- [24] D. Achilles, Ch. Silberhorn, C. Sliwa, K. Banaszek, I. A. Wamsley, M. J. Fitch, B. C. Jacobs, T. B. Pittman, and J. D. Franson. Photon-number-resolving detection using time-multiplexing. *J. Mod. Opt.*, 51(9-10):1499, 2004.
- [25] W. Schleich and J. A. Wheeler. Oscillations in photon number distribution of squeezed states and interference in phase space. *Nature*, 326:574, 1987.
- [26] M. S. Kim, F. A. M. Olivera, and P. L. Knight. Properties of squeezed states and squeezed thermal states. *Phys. Rev. A*, 40(5):2494, 1989.
- [27] A. I. Lvovsky and S. A. Babichev. Synthesis and tomographic characterization of the displaced fock states. *Phys. Rev. A*, 66:011801 (R), 2002.